International Journal of Mass Spectrometry 282 (2009) 38–44

Contents lists available at ScienceDirect

International Journal of Mass Spectrometry

journal homepage: www.elsevier.com/locate/ijms

Modeling and optimization of dual-cylinder image current detector in electrostatic ion beam trap for mass spectrometry

Qi Sun[a,*], Li Ding[b], Changxin Gu[a]

[a] Department of Materials Science, Fundan University, 220 Handan Rd., Shanghai 200433, People's Republic of China
[b] Shimadzu Research Laboratory Shanghai Co. Ltd., 108 Second Kayuan Rd., Shanghai 201201, People's Republic of China

ARTICLE INFO

Article history:
Received 11 November 2008
Received in revised form 3 February 2009
Accepted 4 February 2009
Available online 13 February 2009

Keywords:
Dual-cylinder image current detector
Electrostatic ion beam trap
Mass spectrometry
Numerical electrostatic model

ABSTRACT

In this paper, dual-cylinder image current detector is introduced and simulated using a numerical electrostatic model in the context of electrostatic ion beam trap (EIBT). Being illuminated by the simulation results, the principle of optimizing this new-type detector is proposed, and the configuration of the detector is modified further to improve the signal waveform. The differential current acquired by an optimized dual-cone detector is strengthened more than ten times than that of single-cylinder detector used in the experiment, which is considerable in the process of signal pick-up and the process of signal analysis in mass spectrometry. The simulation results could be used to devise and optimize the image current detector thus to improve the detected signal, and indicate signal analysis (such as FFT) of EIBT for mass spectrometry.

1. Introduction

EIBT (electrostatic ion beam trap) has been invented and developed during the last decade, which stores and manipulates ions with only electrostatic fields [1–4]. When a group of ions is injected into EIBT, they would be trapped and oscillate between the two parallel sets of electrode mirrors with applied voltages, which working principle is similar to that of an optical resonator, and accordingly endows EIBT with another name of ion-trap resonator [5–7]. It has been demonstrated that EIBT is a competent instrument to perform various experiments both in physics and in chemistry, such as life time measurement of metastable state atomic, molecular and negative ions [8–11], electron-impact experiments [12,13], beam dynamics and mass spectrometry [14,15].

In the arrangement of EIBT, a cylindrical detector tube is grounded and mounted between the two mirrors. During a group of ions with certain energy passing through this cylindrical detector, an induced image current could be detected, and based on which the ion charge and ion flight time could be determined. Consequently, EIBT could be used as time-of-flight mass spectrometry, in which the flight path of the ions is multiple folded by electrode mirrors, and thus high resolution of mass analysis is expected.

As the detected current signal with a strengthened intensity is valuable both in the process of signal pick-up and in the process of signal analysis, it has been attempted to improve the intensity of the current signal with optimizing the configuration of the detector.

It was supposed that, with aligning two cylindrical detectors in the path of ion movement, which are insulated from each other and both grounded, a combined differential current signal with strengthened intensity would be expected. This consequence is presumed to be that, the difference of image currents on these two detectors would produce one combined current with doubled intensity because of the symmetrical arrangement.

Based on this assumption, a new-type image current detector is proposed and devised. With the establishment and numerical simulation of an electrostatic model, the initial proposal is validated successfully. Moreover, being illuminated by the simulation results, the configuration of dual-cylinder detector is modified further, and two truncated conical components are adopted to improve the waveform of the signal.

In this paper, a numerical electrostatic model of dual-cylinder image current detector is established to study the principle of this new-type detector, with the concentration to optimize the configuration and acquire improved current signal. The simulation results are also compared and examined with the experimental ones, the two of which agree well. In Section 2 the model is described and in Section 3 the dimensional analysis is preformed. Results and discussion are presented in Section 4, and Conclusions are given in Section 5.

2. Numerical modeling

According to above proposal, a simplified simulation model is adopted, as shown in Fig. 1. The dual-cylinder detector is composed

* Corresponding author. Tel.: +86 21 65643649; fax: +86 21 65643647.
E-mail address: sqhit@fudan.edu.cn (Q. Sun).

1387-3806/$ – see front matter © 2009 Elsevier B.V. All rights reserved.
doi:10.1016/j.ijms.2009.02.002

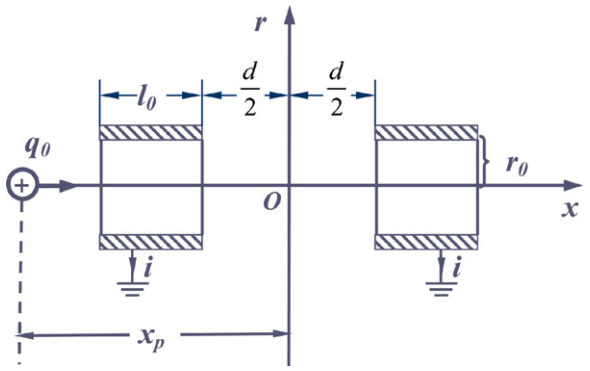

Fig. 1. The schematic configuration of dual-cylinder image current detector.

of two identical cylindrical components, which radius and length are $\boldsymbol{r_0}$ and $\boldsymbol{l_0}$ respectively, and the gap between them is $\boldsymbol{d}$. The quantity of the electric charge that carried by the moving ions is $\boldsymbol{q_0}$, and the ions' position is specified by the coordinate of $\boldsymbol{x_p}$. The thickness of the detector is very thin comparing with its dimension, and has been neglected during the simulation.

In order to simplify the problem, following assumptions are introduced:

(1) the ions are all endowed with exactly the same energy and carrying single charge;
(2) the ions move along the axis of the cylinder, and remain constant velocity during the whole period of simulation, that is, the energy loss during ions' movement is neglected;
(3) The induced charge on the cylinder responds immediately to the moving ions, thus to neglect the signal delay caused by the detecting circuit;
(4) The coulomb repulsion between the ions is not considered in this model.

As both components of the detector are grounded, their potential maintains zero at all time. The potential caused by the moving ions outside is counteracted by that caused by the charge induced on the detector itself. Therefore, at any point x on the detector,

$$\phi(x) = \phi_{induce}(x) + \phi_q(x) = 0 \tag{1}$$

where $\phi(x)$ is the potential at point x, $\phi_{induce}(x)$ is the potential caused by the charge induced on the detector, and $\phi_q(x)$ is that caused by the moving ions outside, and the latter two parts cancel each other entirely.

A numerical method is adopted to acquire the induced charge distribution on the detector. Each cylindrical component is discretized into n segments in x direction, and each segment is specified a certain quantity of induced charge q_i. At the center of jth segment x_j, Eq. (1) becomes

$$\phi(x_j) = \phi_{induce}(x_j) + \phi_q(x_j) = 0 \tag{2}$$

$\phi_{induce}(x_j)$ is contributed by the induced charge from every segment, and thus could be written as

$$\phi_{induce}(x_j) = \sum_{i=1}^{2n} \phi_{ij} = -\phi_{qj} \tag{3}$$

where ϕ_{ij} is the potential at x_j caused by the induced charge on ith segment. With applying Coulomb's law and numerical integral, Eq. (3) could be expressed in the form of q_i, the quantity of induced charge on ith segment,

$$\frac{1}{4\pi\varepsilon_0}\sum_{i=1}^{2n} q_i a_i = -\frac{1}{4\pi\varepsilon_0}\frac{q_0}{r_j} \tag{4}$$

where r_j is the distance between the moving ion and x_j, and the coefficient of a_i could be specified by numerical integral, which dimension is $[1/r]$. With canceling the common factor, Eq. (4) could be simplified into the following form:

$$\sum_{i=1}^{2n} q_i a_i = -\frac{q_0}{r_j} \tag{5}$$

The above equation is linear about charge and distance, and with non-dimensionalization it would become simpler and easier to analysis. Following non-dimensionalized variables are introduced, $X = x/l_0$, $R = r/l_0$ and $Q = q/q_0$, where l_0 is the length of the cylindrical component, and q_0 is the total charge of the moving ions. Thus Eq. (5) becomes

$$\sum_{i=1}^{2n} Q_i A_i = -\frac{1}{R_j} \tag{6}$$

For every segment an equation in the form of Eq. (6) could be established, and a series of linear equations could be set

$$\mathbf{AQ} = \mathbf{B} \tag{7}$$

With solving the above equations, the total induced charge on the first and second component of the detector are

$$Q_1 = \sum_{i=1}^{n} Q_i, \quad Q_2 = \sum_{i=n+1}^{2n} Q_i \tag{8}$$

which rate of change with respect to time is the induced image current of each component.

With reducing the two components of the detector into just one component, this model could simulate the case of conventional single-cylinder detector, and which is performed in the following part to compare with the experimental results.

3. Dimensional analysis

With non-dimensionalization, the form of the equations is simplified, and the range covered by the solution is enlarged. Furthermore, the property of the detector and the principle of detected signal could be elucidated through dimensional analysis. With introducing practical parameters of the detector, the simulated image current signal could be compared with the experimental results.

3.1. Induced image current

As the ion velocity is assumed to be constant, the relation between time t and ion position x_p is

$$x_p = x_0 + v_0 t \tag{9}$$

where x_0 is the starting point of the ions, v_0 is the velocity of the ions, which is determined by the initial energy E_0 and ion mass m.

$$v_0 = \sqrt{\frac{2E_0}{m}} \tag{10}$$

The relation between x_p and non-dimensionalized X_p is $x_p = l_0 \cdot X_p$, thus the relation between dt and dX_p is

$$dt = \frac{l_0}{v_0} dX_p \tag{11}$$

The induced image current between the detector and the ground is

$$I = \frac{dq_{induce}}{dt} \tag{12}$$

As expressed by the non-dimensionalized variables, Eq. (12) becomes

$$I = \frac{q_0 v_0}{l_0}\left(\frac{dQ_{induce}}{dX_p}\right) \tag{13}$$

where (dQ_{induce}/dX_p) is the simulation result with respect to a certain radius $\boldsymbol{R_0}$ and $\boldsymbol{D}$ (that is the ratio of r_0/l_0 and d/l_0), and would not change so long as $\boldsymbol{R_0}$ and $\boldsymbol{D}$ are kept unchanged. From Eq. (13) it is found that the current signal is proportional to q_0 and v_0, and inversely proportional to l_0. If two species of ions are arranged to acquire the same energy E_0, and start to race in the same detector at the same time, the image currents caused by these two groups of ions are

$$I_1 = \frac{q_{01} v_{01}}{l_0}\left(\frac{dQ_{induce}}{dX_p}\right) \tag{14}$$

and

$$I_2 = \frac{q_{02} v_{02}}{l_0}\left(\frac{dQ_{induce}}{dX_p}\right) \tag{15}$$

Thus the ratio of these two current signals is

$$\frac{I_1}{I_2} = \frac{q_{01} v_{01}}{q_{02} v_{02}} = \frac{q_{01}}{q_{02}}\sqrt{\frac{m_2}{m_1}} \tag{16}$$

With different velocity, the two induced current would be detected at different time, thus can be distinguished with different mass and species. With analyzing signal strength, the quantitative analysis could also be performed.

The waveform of the current signal is specified by FWHM (full width at half maximum), and the ratio of these two FWHMs is

$$\frac{FWHM_1}{FWHM_2} = \frac{v_{02}}{v_{01}} = \sqrt{\frac{m_2}{m_1}} \tag{17}$$

Which means the width of the waveform is inversely proportional to the velocity of the moving ions.

With examining Eq. (13) it is also found that, if q_0 and v_0 remain the same, and the configuration of the detector is kept unchanged (i.e., R_0 and D are kept constant), but the size of it is modified, then the detected signal would be halved as the size of the detector doubled. That result would give us some information about the detected current signal when there is an intention to miniaturize or change the size of the detector.

3.2. Energy loss

The resistance of the detecting circuit is assumed to be R, and the energy loss of the ions could be calculated from the heat loss by the circuit resistance, that is $\int I^2 R\,dt$. Suppose the number of ions is N_q, thus the energy loss of each ion is

$$\Delta E = \frac{1}{N_q}\int I^2 R\,dt \tag{18}$$

and with introducing a new variable

$$\Delta E_0 = \int \left(\frac{dQ}{dX_p}\right)^2 dX_p \tag{19}$$

which is non-dimensional and would not change so long as the configuration of the detector is unchanged, and then Eq. (19) becomes

$$\Delta E = \frac{R N_q e_0^2 v_0}{l_0}\Delta E_0 \tag{20}$$

In which $e_0 = 1.61 \times 10^{-19}\ C$ is the elementary charge unit. From Eq. (20) it is found that, for the detector with the same configuration, the energy loss for each ion is proportional to R (the electric circuit resistance), N_q (the number of the moving ions), and v_0 (the velocity of the moving ions), and inversely proportional to the size of the detector.

3.3. Induced current and energy loss with the practical parameters

According to experimental setup [14], l_0 is set to be 7 mm, r_0 is set to be 9 mm. A group of Ar^+ ions with the number of 10^6 and the energy of 4.2 keV are arranged to move through single cylindrical detector. According to Eq. (13), the induced image current is

$$I = 3.276 \times 10^{-6}\left(\frac{dQ}{dX_p}\right) \tag{21}$$

The simulated image current signal is shown in Fig. 2, which is on the order of 1 μA, and the FWHM of the signal is 114 ns. The simulation result is consistent with that of the experiment.

As the resistance of detecting circuit is assumed to be 10 Ω, Eq. (18) becomes

$$\Delta E = 5.274 \times 10^{-24}\Delta E_0 \tag{22}$$

and the relative energy loss of each ion to its initial energy is

$$\frac{\Delta E}{E_0} = 7.848 \times 10^{-9}\Delta E_0 \tag{23}$$

A series of simulations were executed for different R_0, and the results were shown in the Table 1.

It was found from the table that ΔE_0 increases with decreasing R_0, and is on the order of ~1, which makes the relative energy loss of each ion neglectable according to Eq. (23). Simulation results demonstrate that the constant velocity assumption of the ions is reasonable. Thus the ions can be arranged to pass through the detector to and fro many times, and the prolonged path of the ions would improve the resolution of mass spectrometry.

In the following discussion, (dQ/dX_p) is equivalent to current I, and ΔE_0 is equivalent to energy loss ΔE, which would not change so long as the configuration of the detector is unchanged, that is, $\boldsymbol{R_0}$ and $\boldsymbol{D}$ is fixed.

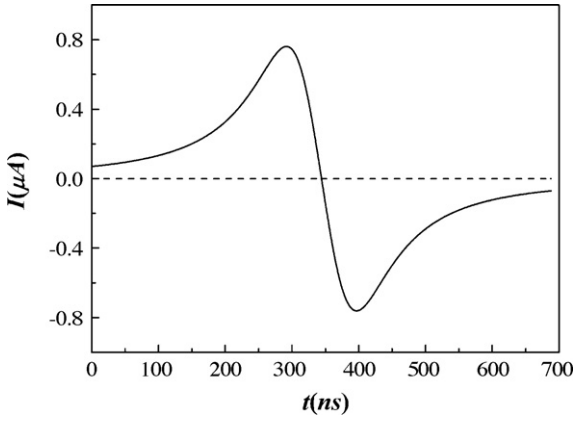

Fig. 2. The simulation result of current signal acquired by single-cylinder image current detector with practical parameters.

Table 1
The energy loss ΔE_0 with different R_0.

R_0 (r_0/l_0)	ΔE_0
0.2	1.3146
0.4	0.7279
0.6	0.4902
0.8	0.3551
1.0	0.2698

4. Simulation results and discussion

4.1. Induced image charge and image current of individual component

The moving ions would induce image charges on both components of the detector, which would distribute self-consistently to compensate the potential caused by the ions outside. Fig. 3 shows the image charge and image current induced on individual component of the detector with $\boldsymbol{R_0} = 1.0$ and $\boldsymbol{D} = 1.0$. It is shown that the electrostatic mutual effect of two components distorted the curve of induced charge and induced current from that of the single-cylinder detector (the curve of the red dashed one).

For the first component, the amount of induced charge reaches its maximum near the middle of the cylinder, which is a little less than that acquired by the single-cylinder detector due to the participation of the second component. After the ions pass the middle of the first cylinder, the induced charge decreases markedly, and reaches its minimum when the ions go out of the second component. The reason for this effect is that, as the ions are mainly shielded by the second one as they passing through, the charge induced with the same sign restrains that on the first component. As a result, the current peak between the two components is almost doubled, while the opposite current peak is slightly influenced, which is almost the same as that acquired with single-cylinder detector.

Because of the symmetrical arrangement of the detector, the first component affects the second one in the same way as shown in Fig. 3(b). As the ions are far away from the detector, the electric effect is mainly shielded by the first component, which restrains the induced charge on the second component to a low level. A steep increase of induced charge appears during the ions passing through the first component and the gap, and accordingly the image current is also intensified in the middle of the two components.

4.2. Differential current signal of the detector

The already strengthened current acquired by individual component of the detector could be combined to form an even stronger one, what needed is to calculate the difference of the two signals. The result is shown in Fig. 4, and it is found that the combined signal is almost doubled. This simulation results shows that such

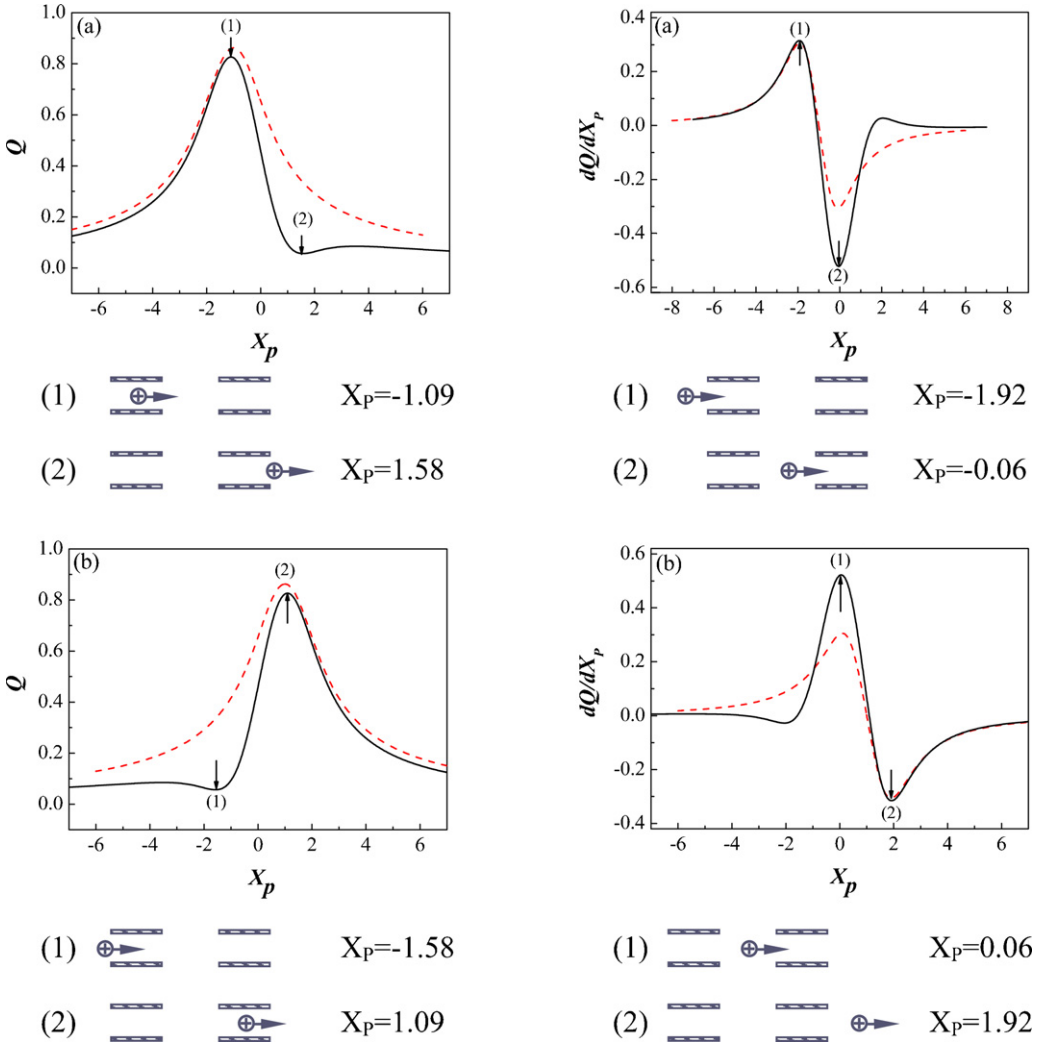

Fig. 3. The image charge (left) and image current (right) induced on individual cylindrical component of the detector with $R_0 = 1.0$ and $D = 1.0$. (a) The first component and (b) the second component. The peak of the curve is labeled in the figure, and the corresponding location of the ion relative to the detector is also schematically showed.

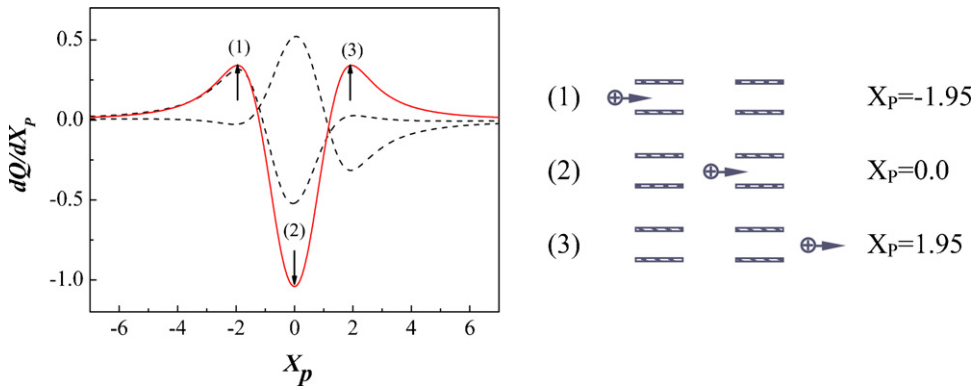

Fig. 4. The combined differential current acquired by dual-cylinder detector with R_0 = 1.0 and D = 1.0.

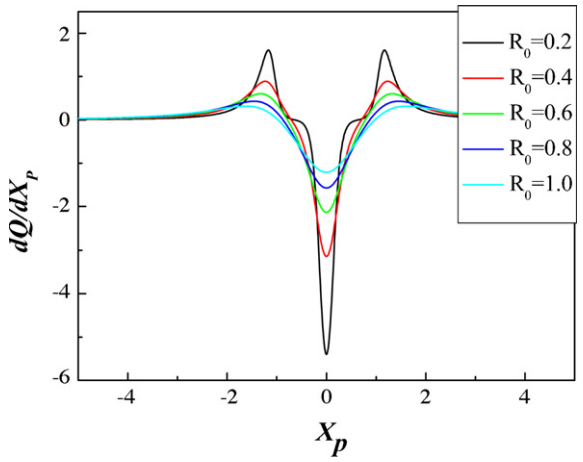

Fig. 5. The influence of R_0 on the differential current of dual-cylinder detector with D = 0.2.

an arrangement of the detector would intensify the current signal almost four times stronger, which is quite considerable in mass analysis technique.

Except the strengthened differential current, there are two current peaks with the opposite direction on both sides of the detector. The latter two are almost of the same level as the image current acquired with single-cylinder detector, but the former is increased by almost four times.

4.3. Influence of the radius R_0

A series of simulation with varying $\boldsymbol{R_0}$ is performed, in which $\boldsymbol{D}$ is fixed to be 0.2, and the simulation result of the differential current is shown in Fig. 5. It is found that with decreasing the radius of the cylinder, both the differential current signal and the opposite current signal are increased markedly, and the signal width becomes narrower. The radius also plays an important role in the case of single-cylinder detector, and a strengthened image current is also expected with decreasing radius R_0. However, with the configuration of dual-cylinder detector, the image current acquired by individual component is almost doubled between the two components, and the combined differential current is doubled once more.

Table 2
The influence of $\boldsymbol{R_0}$ on differential current signal and the energy loss.

$\boldsymbol{R_0}$ ($\boldsymbol{r_0}$/$\boldsymbol{l_0}$)	$(dQ/dX_p)_{max}$	FWHM	ΔE_0
0.2	5.398	0.34	5.176
0.4	3.138	0.56	2.870
0.6	2.133	0.78	1.840
0.8	1.571	0.95	1.238
1.0	1.209	1.1	0.864

The relative signal parameters and the energy loss is presented in Table 2, which shows the peak value of differential current $(dQ/dX_p)_{max}$, the shape of the current signal FWHM, and the energy loss of the ions ΔE_0. As $\boldsymbol{R_0}$ decreases form 1.0 to 0.2, the peak value of the differential current increases near five times from 1.2 to 5.4, and as the radius becomes smaller, the strengthening effect becomes more evident. The strengthened signal certainly corresponding to a higher energy loss, but even the biggest one of them is very small, and could be neglected.

4.4. Influence of the gap D

A series of simulation with varying $\boldsymbol{D}$ is performed in two cases, one which $\boldsymbol{R_0}$ is smaller than $\boldsymbol{D}$, and the other which $\boldsymbol{R_0}$ is larger

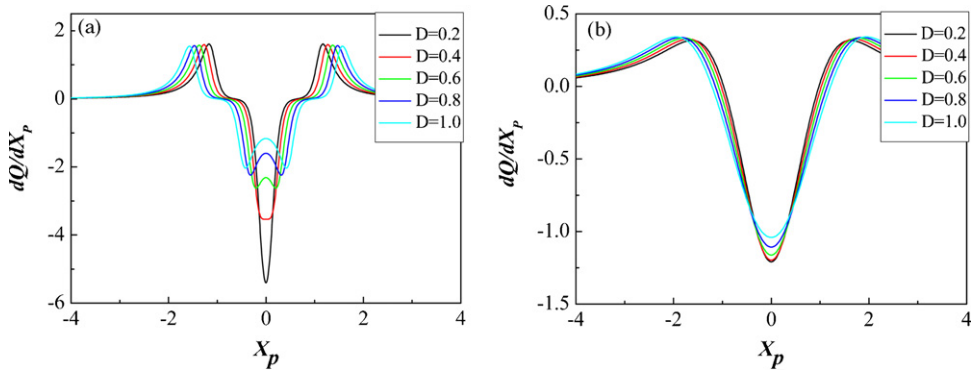

Fig. 6. The influence of D on the differential current of dual-cylinder detector (a) R_0 = 0.2 and (b) R_0 = 1.0.

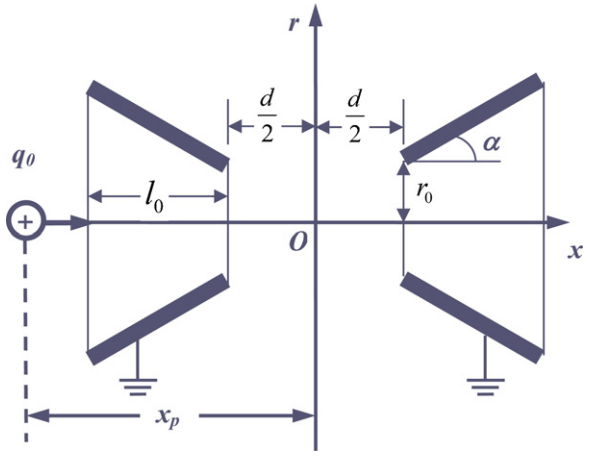

Fig. 7. The schematic configuration of the modified dual-cone image current detector.

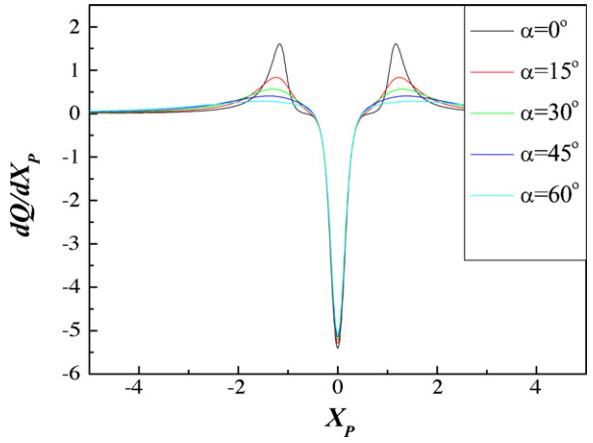

Fig. 8. The influence of conical angle α on the differential current of dual-cylinder detector with $R_0 = 0.2$ and $D = 0.2$.

than $\boldsymbol{D}$. The simulation result of the first case is shown in Fig. 6(a), in which $\boldsymbol{R_0}$ is 0.2. It is found that with increasing the gap between the two components, the differential current signal is weakened evidently, and two peaks appear in the combined curve. As the radius $\boldsymbol{R_0}$ decreasing, the image current of individual component appears more nearer to its edge, and the current signals between the two components misalign in a wider gap. As a result, the differential current signal is not intensified adequately. The simulation result of the second case is shown in Fig. 6(b), in which $\boldsymbol{R_0}$ is 1.0. In this case, increasing the gap $\boldsymbol{D}$ only decreases differential current slightly, and makes FWHM a little wider.

Summarizing the above simulation results, it is found that $\boldsymbol{R_0}$ is the key factor that determines the strength of the signal, and the gap $\boldsymbol{D}$ is the key factor that determines whether the two strengthened signals in the gap is aligned well. This principle is also demonstrated in Fig. 6(b), that in the case of $\boldsymbol{D} \leq \boldsymbol{R_0}$, varying $\boldsymbol{D}$ with fixed $\boldsymbol{R_0}$ makes little difference in the current signal. Therefore, in the optimization of this new-type detector, the gap $\boldsymbol{D}$ between the two components should not be larger than the radius $\boldsymbol{R_0}$.

4.5. Influence of the conical angle α in the modified dual-cone image current detector

For this new type detector, three peaks appear in the current curve, one differential current peak, and two opposite current peaks. The latter two would increase the noise level of the background, and interfere with signal analysis. Based on the simulation results, the detector is modified further with an aim to alleviate the strength of the opposite current. Fig. 7 shows the schematic configuration of the dual-cone image current detector, in which the cylindrical components is replaced by the truncated conical components with their apexes pointing to each other. Conical angle $\boldsymbol{\alpha}$ is introduced to describe the shape of this detector, and $\boldsymbol{r_0}$ is the radius of the truncated cone on the apex side.

Differential current of this detector is simulated with varying α form 0° to 60° as shown in Fig. 8, in which $\boldsymbol{R_0} = 0.2$ and $\boldsymbol{D} = 0.2$. It is shown from the figure that the signal of differential current is slightly decreases with increasing the conical angle, but the opposite current is alleviated remarkably.

This point is clearly shown in Table 3. As the conical angle increase from 0° to 60°, the peak value of differential current only decreases from 5.4 to 5.06, less than ten percents, and FWHM is almost the same for all these cases. But the peak value of the opposite current decreases from 1.61 to 0.28 by more than five times. Because of the distinct alleviation of the opposite current, the energy loss is decreases evidently.

Table 3
The influence of $\boldsymbol{\alpha}$ on current signal and the energy loss.

α	$(dQ/dX_p)_{max}$	FWHM	ΔE_0	$-(dQ/dX_p)_{max}$
0°	5.398	0.34	5.176	1.61
15°	5.29	0.34	4.383	0.84
30°	5.21	0.34	3.997	0.57
45°	5.14	0.33	3.714	0.41
60°	5.06	0.33	3.467	0.28

It should be noticed that the conical angle could not be adjusted arbitrarily, but is limited by the size of the electrostatic trap. And as the conical angle grows larger, the capacitance effect between these two components would interfere with the electric induction effect, and destroy the detection signal. Consider a moderate angle of 45°, and it is found that the combined current decreases a little from 5.39 to 5.14, but the opposite current decreases from 1.61 to 0.41 which is quite remarkable.

4.6. Optimization of the configuration of the detector

Based on the simulation results, several principles should be followed in the optimization of dual-cone image current detector. They are

(1) In order to acquire signal with high intensity, the radius $\boldsymbol{R_0}$ should be small.
(2) In order that the current of the two components aligns well, the gap $\boldsymbol{D}$ between them should be less than $\boldsymbol{R_0}$.
(3) In order to alleviate the opposite current signal, certain conical angle should be selected.

The optimization of these three parameters is also limited by the machining precision, the size of the electrostatic trap, and the loss of the ions.

In order to reduce the ion loss, the practical radius $\boldsymbol{r_0}$ is set to be 2 mm, and the length of the conical component is selected to be 10 mm. According to the design principle, the gap $\boldsymbol{d}$ between the two conical components is also set to be 2 mm. The conical angle α is selected to be 45°. With introducing these practical parameters, and according to Eq. (21), differential current acquired by this optimized new-type detector is on the order of 10 μA, FWHM of the signal is 23.9 ns, and the relative energy loss of each ion is $\Delta E/E_0 = 1.74 \times 10^{-8}$. Whereas the current signal of single-cylinder detector used in the experiment is on the order of 1.0 μA.

5. Conclusion

With the simulation results of dual-cylinder image current detector, the following conclusion is deduced

(1) The mutual effect of the two components in the detector strengthened the image current that appears in the gap, and with calculating the difference of these two image currents, the differential current signal is intensified once more.
(2) With decreasing the radius R_0, the strength of the signal is remarkably increased, which shows that R_0 plays a key role in determining the strength of the signal.
(3) When $D \geq R_0$, the increase of D would make the combined single split into two peaks, which is caused by the misalignment of the two current signals in the gap.
(4) On the other hand, when $D \leq R_0$, the increase of D would not cause the above effect, but decrease the combined current slightly.
(5) With increasing the conical angle of the conical component in the detector, the strength of the opposite current is evidently decreased, but the differential current is only influenced slightly.
(6) The current signal acquired by an optimized dual-cone detector is strengthened more than ten times than that of the single-cylinder detector, which is considerable in signal pick-up and analysis of mass spectrometry.

References

[1] D. Attia, D. Strasser, O. Heber, M.L. Rappaport, D. Zajfman, Nucl. Instrum. Meth. A 547 (2005) 279.
[2] M. Dahan, R. Fishman, O. Heber, M.L. Rappaport, N. Altstein, D. Zajfman, W.J. van der Zande, Rev. Sci. Instrum. 69 (1998) 76.
[3] D. Zajfman, D. Strasser, O. Heber, S. Goldberg, A. Diner, M.L. Rappaport, Nucl. Instrum. Meth. A 532 (2004) 196.
[4] T. Suzuki, Y. Yamauchi, Nucl. Instrum. Meth. A 562 (2006) 53.
[5] H.B. Pedersen, D. Strasser, B. Amarant, O. Heber, M.L. Rappaport, D. Zajfman, Phys. Rev. A 65 (2002) 042704.
[6] H.B. Pedersen, D. Strasser, O. Heber, M.L. Rappaport, D. Zajfman, Phys. Rev. A 65 (2002) 042704.
[7] H.B. Pedersen, D. Strasser, S. Ring, O. Heber, M.L. Rappaport, Y. Rudich, I. Sagi, D. Zajfman, Phys. Rev. Lett. 87 (2001) 055001.
[8] A. Wolf, K.G. Bhushan, I. Ben-Itzhak, N. Altstein, D. Zajfman, O. Heber, M.L. Rappaport, Phys. Rev. A 59 (1999) 267.
[9] L. Knoll, K.G. Bhushan, N. Altstein, D. Zajfman, O. Heber, M.L. Rappaport, Phys. Rev. A 60 (1999) 1710.
[10] K.G. Bhushan, H.B. Pedersen, N. Altstein, O. Heber, M.L. Rappaport, D. Zajfman, Phys. Rev. A 62 (2000) 012504.
[11] O. Heber, R. Golser, H. Gnaser, D. Berkovits, Y. Toker, M. Eritt, M.L. Rappaport, D. Zajfman, Phys. Rev. A 73 (2006), 060501(R).
[12] O. Heber, P.D. Witte, A. Diner, K.G. Bhushan, D. Strasser, Y. Toker, M.L. Rappaport, I. Ben-Itzhak, N. Altstein, D. Schwalm, A. Wolf, D. Zajfman, Rev. Sci. Instrum. 76 (2005) 013104.
[13] L.H. Andersen, O. Heber, D. Zajfman, J. Phys. B: At. Mol. Opt. Phys. 37 (2004) R57.
[14] D. Zajfman, Y. Rudich, I. Sagi, D. Strasser, D.W. Savin, S. Goldberg, M.L. Rappaport, O. Heber, Int. J. Mass Spectrom. 229 (2003) 55.
[15] K.G. Bhushan, S.C. Gadkari, J.V. Yakhmi, V.C. Sahni, Rev. Sci. Instrum. 78 (2007) 083302.